JOURNAL OF MATERIALS SCIENCE **34** (1999) 5945 – 5953

Structural studies of ideal organic-inorganic nanocomposites by high resolution diffractometry and NMR spectroscopy techniques

M. LARIDJANI
Laboratoire de Physique des Solides-Bât. 510, Université Paris-Sud, 91405 Orsay-France

E. LAFONTAINE
DGA/CREA, 16 bis Avenue Prieur de la Côte d'Or, 94114 Arcueil Cedex-France

J. P. BAYLE, P. JUDEINSTEIN*
Laboratoire de Chimie Structurale Organique (UPRESA CNRS 8074)-Bât. 410, Université Paris-Sud, 91405 Orsay-France
E-mail: pjudeins@icmo.u-psud.fr

Hybrid organic-inorganic materials, silica-poly(ethylene glycol) (PEG) blends, were prepared by the sol-gel process from mixtures of tetraethoxysilane and PEG of low molecular mass. The synthesis scheme (acidic [HCl] or nucleophilic [NH_4F] catalysis) influences the structure of these materials and consequently their properties. Two different methods were used to investigate the structure of these blends: a) X-ray diffraction techniques; b) ^{29}Si NMR spectroscopy. A new x-ray diffractometry technique identifies precise interference functions and radial distribution functions of these blends. The comparison of predicted radial distribution functions of the Bell and Dean's physical model refined by Gaskell with the radial distribution function obtained from this technique is implemented to identify the structure of these blends. Analysis by amorphography has identified the existence of SiO_2 silica grains and provides only about the positional disorder of these grains in continuum random network. The NMR spectroscopy discriminates the different silicon sites and demonstrates the changes of the morphology and structure when the nature of the catalyst is modified. These results indicate that the structure of non-crystalline SiO_2 aggregates inside nanocomposites differs from fused glass by their compositional disorders. These nanocomposites could be described as an agglomerate of SiO_2 objects with the pores filled by disordered polymer chains. When these materials are obtained under acidic conditions, the polymer chains are linked to the SiO_2 grains forming an *ideal composite*. *© 1999 Kluwer Academic Publishers*

1. Introduction

The design of organic-inorganic nanocomposites is a fascinating topic for science and technology and many applications are expected in the fields of optics, mechanics, iono-electronics, biosensors, membranes [1].

Nanocomposite materials are prepared by the sol-gel process. Inorganic molecular precursors (silicon alkoxides) and polymer (poly(ethyleneglycol), PEG) are mixed and a solid matrix is obtained by hydrolysis-condensation [2]. These reactions could be performed using different catalysis conditions. These materials, also named "hybrids", have been reported as diphasic media. This diphasic morphology was recognized using experimental techniques such as scanning electron microscopy [3], atomic force microscopy [4] or small angle X-ray (SAXS) [5, 6]. It is a known fact that these techniques characterize material "granulity" independently from the atomic structures of these nanograins [7]. It was reported that these silica nanograins are wrapped by the polymer phase [8]. However, the *atomic structure* of these nanograins and of the polymer phase in such mixtures is still not known.

In this paper, a new X-ray diffraction technique, the anomalous diffractometry, has been used to determine the *atomic structures* of nanograins and polymer phase while the chemical local order of silicon sites have been established by ^{29}Si solid state NMR. Using these two techniques, it can be shown that the morphology and the atomic structure both are affected by varying the catalysis conditions. The effects of the synthesis conditions, especially those coming from the nature of the catalyst which could be acidic (hydrochloric acid; HCl) or

---

* Author to whom all correspondence should be addressed.

0022–2461

nucleophilic (ammonium fluoride; NH_4F) are discussed.

2. Experimental sections

2.1. Synthesis

All chemical reagents were purchased at Fluka or Aldrich companies; these includes tetraethoxysilane ($Si(OC_2H_5)_4$; TEOS) as silica precursor and poly (ethylene)glycol ($H(OCH_2CH_2)_xOH$; PEG_n) where n is the molecular weight ($n = 200$, 300 and 600) as organic polymer; hydrochloric acid and ammonium fluoride (NH_4F) as catalysts. Deionized water was used in all experiments.

The following nomenclature was applied for the materials: A_n; where A represents the type of catalyst, H or N respectively for acidic (HCl) or nucleophilic (NH_4F) catalysis and n the molecular weight of the PEG. For all materials, the catalyst ratio [catalyst]/[Si] has been kept constant and equal to 10^{-3}, the hydrolysis ratio was chosen to be $[H_2O]/[Si] = 10$ and the silica content was 23 wt %.

The synthesis of the representative H_{200} material is described as follows: TEOS (1 g, $4.8 \cdot 10^{-3}$ mol) was added to PEG_{200} (0.97 g, $4.8 \cdot 10^{-3}$ mol) and 0.86 g of water-catalyst solution ($4.8 \cdot 10^{-2}$mol H_2O, $4.8 \cdot 10^{-6}$ mol HCl) under vigorous stirring. One ml of EtOH was then added and the mixture was heated to 60 °C and stirred for 10 min. The liquid was cast in an open air PTFE vessel at room temperature for two days. The samples were aged for 5 days at 80 °C, then 60 °C under vacuum (10^{-2} mm Hg) for three days and the solvents allowed to evaporate. Transparent monolithic materials were obtained for acidic catalysis, while white powders were obtained when NH_4F was used as a catalyst.

2.2. X-ray diffraction techniques

2.2.1. The Guinier camera

X-ray patterns of each samples were obtained in a vacuum with a sensitive photographic method using a monochromatic X-ray beam at the Cu K_α wavelength. Because of the high contrast of the X-ray diagrams, the glassy state of each sample can be checked easily by this technique.

2.2.2. X-ray diffractometry

The diffracted intensity, $I(K)$ (K is the scattering vector, $K = 4\pi \sin\theta/\lambda$), was obtained by a novel design which was modified according to the X-ray source and the sample shape. This novel diffractometer can be adapted to the parallel beam of a high intensity source (rotation-target diffraction tube or synchrotron radiation) [9]. The diffractometer consists of three main parts: a goniometer, an energy calibration and data acquisition with a processing software. In transmission and reflection geometry, the goniometer can be used for θ–2θ scanning with a resolution $\theta = 0.001°$. The parallel beam is obtained by a slit system proposed by Guinier *et al.* [10] for the small angle scattering technique. Hence, the scattered radiation for a very small Bragg angle, θ, is not overshadowed by direct beam. The following section discusses the usefulness of such an option for new materials.

Depending on the information required from the samples, the geometrical condition and optical arrangements of the diffractometer can be optimised. In this special set-up, the goniometer can be used in dispersive and non-dispersive modes. In the dispersive mode, a polychromatic component of x-ray radiation is used, θ and 2θ can be fixed. In the non-dispersive mode, the monochromatic component of x-ray radiation is used in order to obtain x-ray diagrams with different wavelengths, in the same experiment. The energy selection can be performed by two different procedures. The first procedure is to use a flat monochromator providing rapid tunability over a white spectrum. The second procedure is performed by a scattered beam from a substance that can be selected by a programmed multichannel software as an energy window.

We have used a non-energy dispersive technique using high intensity, different wavelengths and a parallel beam to obtain the x-ray patterns of the different nanocomposites. This technique facilitates the important background and Compton scattering corrections for obtaining high quality x-ray diffraction patterns with very high resolution. The parallelism of incident x-ray beams and the geometry of the diffractometer help to eliminate several corrections such as the effect of the sample size or the effect of sample shape.

This ease of wavelegth selection allows us to acquire the patterns with a chosen wavelength, consequently permitting an easy absorption correction and Compton correction for reflection and transmission geometries. This possibility results in obtaining a high quality interference function with a very high range of K.

It is well known that such an interference intensity can be registered from the correlation of the first and second atomic shells, especially in disordered materials such as nanocomposites. But the intensity of interference beams beyond the second shell is not very high specifically for the second phase of this substance (a polymer with very light atoms). Therefore the aberration can be cause of error in analysing the x-ray pattern.

In order to separate fluorescent and incoherent radiation from the coherent component $I_c(K)$, the scattered beam is recorded by a protoype energy dispersive detector which is connected to a preamplifier and a pulse processor. The pulse processor is a sophisticated signal processing unit which provides linear amplification, noise filtering, pulse pile-up and life time rejections. The combination of these functions is an essential prerequisite for achieving accurate x-ray analysis of noncrystalline materials. The pulses are accumulated in a multichannel analyser interfaced with a computer. The solid state detector has an energy resolution of 150 eV at 8 keV and 230 eV at 20 keV. Such high resolution in energy not only permits the elimination of fluorescence radiation from the sample but it also partially removes the incoherent Compton scattering.

This experiment was mounted on a rotating target Rigaku of an Ag x-ray source. In the present study,

$\lambda_{K\alpha} = 0.5609$ Å and $\lambda_{K\beta} = 0.4907$ Å wavelengths were used for X-ray analyses. The sample was scanned from $2\theta = 1^\circ$ to 90° (i.e. from $K = 0.4$ Å^{-1} to 15 Å^{-1}) in transmission geometry and from $2\theta = 1^\circ$ to 140° (i.e. from $K = 0.4$ Å^{-1} to 20 Å^{-1} for $K\alpha$ and 24 Å^{-1} for $K\beta$) in reflection geometry. The value of $K = 24$ Å^{-1} can be considered as an optimum for analysing interference function with respect to other analytical parameters.

Hence, the part of the diagram $[2\theta < 60^\circ]$ obtained by transmission and another part of the diagram $[2\theta > 60^\circ]$ obtained by reflection geometry were used to achieve a more precise $J(K)$ interference function, $J(K) = I_c(K)/Nf^2(K)$ was obtained by scaling the atomic form factor $f(K)$ on the large K data, where N is the number of atoms. The small errors in the normalization of $J(K)$ or more likely of the reduced interference function, $F(K) = K[J(K) - 1]$ were detected and corrected, with the help of the low K data in such a way that below the first correlation peak, the radial distribution function, $W(r) = (r(P(r) - 1) = (2\pi^2\rho_0)^{-1}\int_0^{K\,\max} F(K)\cdot \sin Kr \cdot dK$ would have a slope of -1 (i.e. below this peak there is a probability $P(r) = 0$ to find an atom at a distance of r from a reference atom) [11]. This novel design and the change in correction paramaters such as density have resulted in achieving the slope value of -1. Further details have been described in [12].

2.3. Solid-state ^{29}Si NMR

Solid state NMR spectra were recorded on a Bruker MSL-200 spectrometer at 39.73 MHz for ^{29}Si. The samples were filled in fused zirconia rotor fitted with Kel-F caps and spun at 4 kHz at the magic angle (54.7°). ^{29}Si chemical shifts were referenced relative to the TMS (0 ppm), which was used as an external reference. CP-MAS (Cross Polarization-Magic Angle Spinning) spectra were obtained using a cross-polarization sequence and broadband high power decoupling during acquisition. For these experiments, the NMR parameters were a 20 s recycle delay, a 5 ms mixing time and a 4.1 μs proton 90° pulse. HP-MAS (High Power decoupling-Magic Angle Spinning) spectra were recorded using permanent broad band high power ^{1}H decoupling with a recycle delay of 60 s. The 90° silicium pulse was equal to 6 μs.

3. Results and discussion

3.1. Sample characterization and atomic structural determination

3.1.1. Characterization

All the samples were first verified by the Guinier camera. Fig. 1 shows a series of Guinier patterns of nanocomposites which were prepared by using the two catalysts: acidic (HCl, Fig. 1a,b)) and nucleophilic (NH_4F, Fig. 1c–e)). These two patterns are rather different. Both of them present similar diffusive rings, which are characteristic of amorphous compounds, while a strong and narrow peak (called pre-peak) is observed only for the material prepared under acidic catalysis in the smaller angle region, prior to the first principal diffused halo at $2\theta \cong 11.74$ Å ($K = 0.9$ Å^{-1}). The two materials prepared under acidic conditions (with PEG_{200} and PEG_{300}) show a similar diagram with a pronounced pre-peak, while those prepared under nucleophilic catalysis (with PEG_{200}, PEG_{300} and PEG_{600}) have only broad and diffuse halos. The presence (or absence) of pre-peak in the x-ray diffraction patterns distinguishes between the two different atomic structures obtained after acidic or nucleophilic synthesis conditions. However, from these diagrams, the incorporation and the nature of each phase is not really clear in these type of compounds.

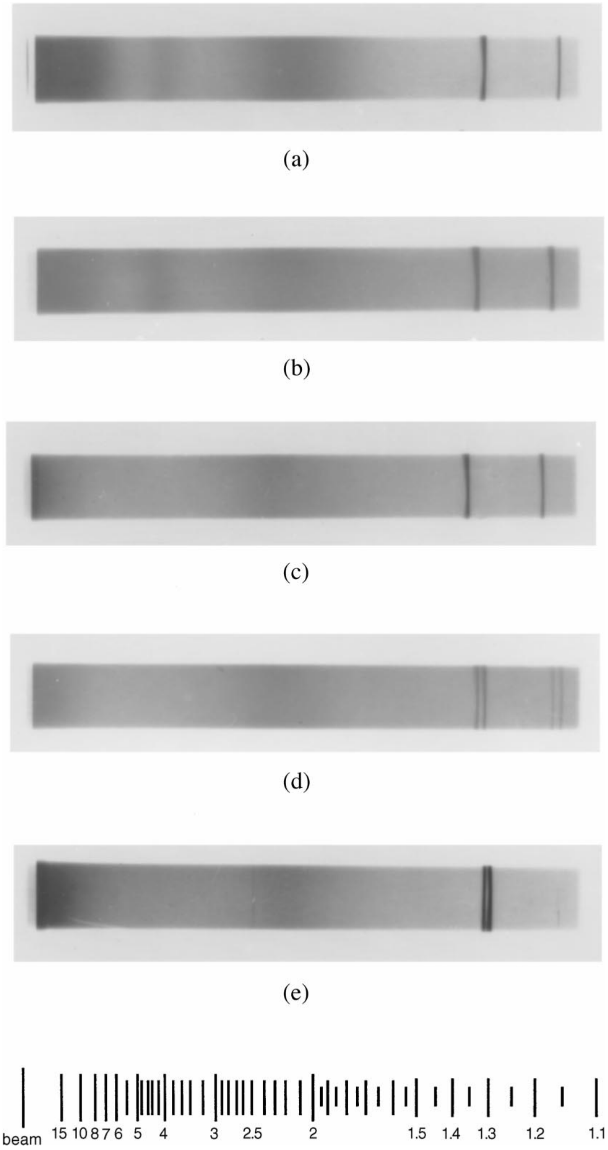

Figure 1 Guinier patterns of five nanocomposite samples obtained under : a) acidic catalysis (HCl), PEG_{200}; b) acidic catalysis (HCl), PEG_{300}; c) nucleophilic catalysis (NH_4F), PEG_{200}; d) nucleophilic catalysis (NH_4F), PEG_{300}; e) nucleophilic catalysis (NH_4F), PEG_{600} (sharp lines come from aluminium which was used as an internal reference). [d] spacings in Å.

3.1.2. Anomalous diffractometry

To identify the provenance of these pre-peaks and halos, X-ray diffraction patterns of pure polymers, liquid and solid, (PEG_{200} and PEG_{1000}) have been recorded using anomalous diffractometry and the representative

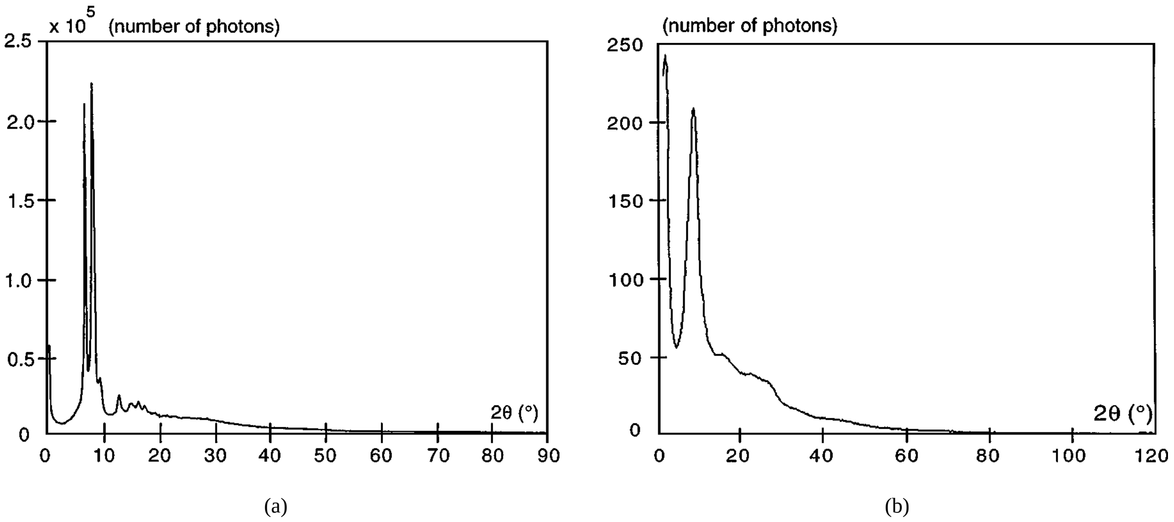

(a) (b)

Figure 2 a) X-ray pattern $I_c(2\theta)$ of solid PEG_{1000} recorded at room temperature ($T = 22\,^\circ C$). Contrary to the X-ray pattern of liquid PEG, there are sharp lines superimposed on the broad difuse rings. This type of pattern can be numerically resolved into broad diffuse rings and sharp lines (cf. Fig. 6); b) X-ray pattern $I_c(2\theta)$ of nanocomposite obtained in acidic catalysis (HCl).

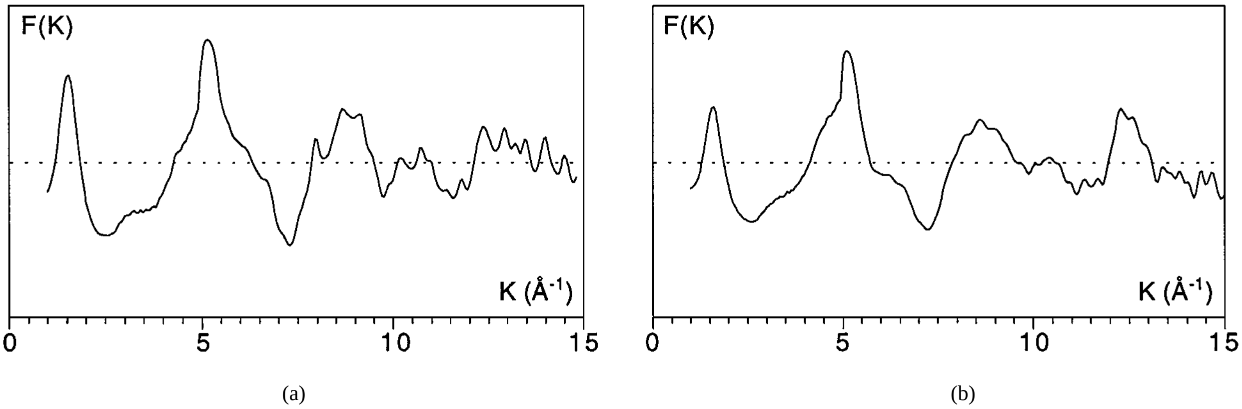

(a) (b)

Figure 3 Reduced interference functions, $F(K)$, for nanocomposites obtained under a) acidic (HCl) catalysis; b) nucleophilic (NH_4F) catalysis.

diagram for PEG_{1000} (at $T = 22\,^\circ C$) is presented on Fig. 2. When the sample is solid, typical lines are superimposed on large halos, while only broad halos of low intensity are observed when the PEG is liquid. On the other hand x-ray patterns of different nanocomposites shows large halos without appearance of any fine lines (Fig. 2b) as it can be observed in x-ray patterns of pure solid PEG Fig. 2a. The absence of sharp lines, in first approximation indicates the atomic rearrangement of PEG. Therefore, because of the low scattering factor of the polymer, we can assume that SiO_2 has a major contribution to the intensity of the X-ray diagram. *It can be suggested that the observed breadth of diffraction patterns can be derived from microcrystallites or the random array model.* In order to interpret these patterns, the total interference function have been implemented to identify the atomic arrangement of atoms responsible for diffuse patterns.

3.2. Atomic structure (positional atomic arrangement)

3.2.1. The reduced interference function, F(K)

Another approach used to describe the atomic arrangement of amorphous nanocomposites is the determination of the $W(r)$ functions. In our previous studies [11], this technique has been referred as amorphography. Such a technique has been used for determining interatomic distances, short range order (SRO), medium range order (MRO) and the number of the neighbouring atoms of the atomic shells inside the different compounds. This technique requires high quality interference functions, $F(K)$.

The reduced interference functions, $F(K)$, of 5 samples prepared under different synthesis conditions have been analyzed, derived from $I_c(2\theta)$ (acidic catalysis, PEG 200 and 300; nucleophilic catalysis, PEG 200, 300 and 600) Fig. 2b. These $F(K)$ curves look rather similar and they are presented in Fig. 3. The peak positions in the different samples are almost identical but certain details, such as the profile of the principal peak, the presence or the absence of the pre-peak and different shoulders on the second and third peaks are slightly different. These differences indicate the variation of “degree of disorder” in different types of nanocomposites and is related to the mode of preparation.

3.2.2. The reduced radial distribution function W(r)

In order to obtain more structural information from the various nanocomposites, the interference functions obtained with Ag K_α were analyzed by Fourier transform.

TABLE I Interatomic distances measured in nanocomposites samples and derived from scientific literature

	Si–O 1st (Å)	O–O 1st (Å)	Si–Si 1st (Å)	Si–O 2nd (Å)	O–O 2nd (Å)	Si–Si 2nd (Å)	Ratio 1st distances:[a] [O–O]/[Si–O]
This work HCl catalyst $\lambda = 0.5609$ Å	1.52	2.49	3.05	3.75	4.13	5.0	1.638
This work NH_4F catalyst $\lambda = 0.5609$ Å	1.60	2.62	3.06	3.80	4.09	5.0	1.637
Experimental X-ray glass, Mozzi-Warren [13] $\lambda = 1.542$ Å, $\lambda = 0.6147$ Å	1.62	2.65	3.12	3.7[b]	4.15	5.12	1.635
Theoretical, glass Mozzi-Warren model [17]	1.638	2.666	3.0	—[c]	4.09	5.07	1.627
Theoretical, glass Bell-Dean model [19]	1.57	2.58	3.15	3.75	4.2	5.1	1.643
Experimental X-ray diffraction of glass Henninger *et al.* [18] $\lambda = 0.71$Å	1.55	2.5(5)	3.07	—[c]	3.95	—[c]	1.645
Experimental neutron diffraction of glass Henninger *et al.* [18] $\lambda = 0.797$ Å	1.59	2.62	3.22	3.7	4.09	5.03	1.647

[a] Tetrahadron ratio.

[b] Not mentioned in the text, but appears as a tiny shoulder on the experimental curve.

[c] Missing in pair correlation functions.

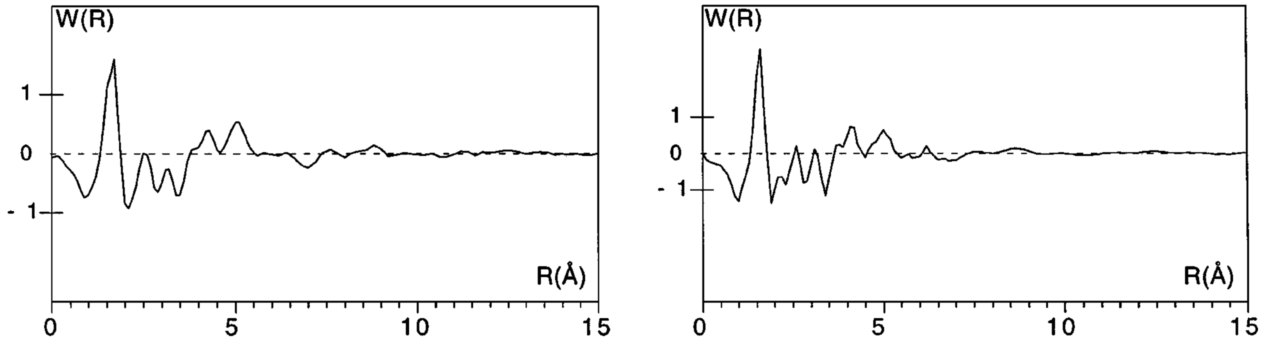

(a)

(b)

Figure 4 Reduced radial distributions, $W(r)$, derived from Fig. 3 for nanocomposites obtained under a) acidic (HCl) catalysis; b) nucleophilic (NH_4F) catalysis.

Fig. 4 shows the reduced radial distributions, $W(r)$, derived from $F(K)$ for the 2 samples (one obtained by acidic catalysis and other group obtained by nucleophilic catalysis). These functions present maxima which are characteristic of the different pair *interatomic distances*. The five samples of nanocomposites give rise to atomic radial distribution functions with substantial similarities. Six maxima corresponding to the different atomic distances can be observed for these different samples. The first maximum is characteristic of the shorter distance corresponding to the silicon-oxygen pair, with lengths of 1.52 and 1.60 Å, respectively for HCl and NH_4F catalysis conditions. The second peak located respectively at $r = 2.49$ and 2.69 Å can be identified as an O–O atomic pair.

The ratio of the second $W(r)$ maxima to the first one ($2.49/1.52 = 1.638$ and $2.62/1.60 = 1.637$) are the same in both samples and correspond exactly to what is expected for regular tetrahedral bonding (i.e. $\sqrt{8/3} = 1.633$). This ratio was already observed in a sample of pure fused quartz (SiO_2) validating the refine tetrahedal structural model proposed by R. L. Mozzi and B. E. Warren for vitreous silica [13, 17] (Table I). Therefore, the silica nanograins inside these materials are based on tetrahedral structural SiO_4 molecular units, as was reported in the structural studies of all the different amorphous and crystalline forms of silica. In these networks, each silicon atoms are tetrahedrally surrounded by four oxygen atoms. However, we should note that in these samples the Si–O bond lengths are very short in regard to those which are reported for *amorphous* silica glasses and are generally in the range of 1.57–1.62 Å as it was recently reported from neutron scattering [14] or using high energy x-ray beam [15]. Such shortening has been already measured by Ohsaki *et al.* in some thin films of SiO_2 prepared by sol-gel process [16]. They used high energy electron diffraction technique and observed that shorter bond lengths are observed for thin films, down to 1.54 Å for 4 Å thick films. This feature could be related to the higher number of surface Si–O bonds when film thickness is decreasing, (leading also to numerous O–H bonds). Thus, in our samples, the short bond lengthes observed in SiO_2-PEG samples prepared in acidic conditions could be related to the smaller size of the silica nanograins and larger interface area.

The third peak ranges in the distance of $r = 3.05$–3.09 Å for the different samples, which logically corresponds to the silicon-silicon contribution. Regarding this bond length, the Si–O–Si bond angle,

α, can be assumed in average to be about 180° ($2 \times 1.52 = 3.04$ Å) for the sample obtained in acidic conditions and less than 180° for NH_4F catalysis. The radial distribution functions of these samples present three other well resolved maxima and beyond these peaks, the oscillations vanish. The disappearance of these oscillations beyond 7 Å indicates that there is no evidence of long range ordering in these grains. It seems, then, that the atoms of these grains have a mean position which ressemble the specific points of the network described by the continuum random model (C. R. N.) proposed by Mozzi and Warren [17]. The structures of these grains are identified, meaning that two distances at $r = 4.13$ and 5.12 Å are expected from this model and these two maxima can be contributed to the mixture of all types of pairing, as they were proposed for fused SiO_2. However, this model does not predict the shoulder at 3.7 Å observed in our experimental $W(r)$ curves (Fig. 4). This shoulder cannot be considered as an experimental artifact, and also cannot be neglected in the global interpretation of atomic structure. This kind of a shoulder has been observed in other experimental radial distribution functions such as the $W(r)$ functions proposed by Henninger *et al.* [18]. In this current work, such a shoulder appears as a well resolved maximum. On the other hand, the distance of $r \approx 3.7$ Å is a signature of the crystalline form of SiO_2 (β-cristoballite or tridymite) and in this case comes from the second Si–O distance. Nevertheless, the microcrystallite model can not be proposed for atomic arrangement of these grains due to the absence of any long-distance maximum and the vanishing oscillations of $W(r)$ beyond 7 Å (see Fig. 4).

The theoretical continuum random network (C.R.N.) refined by Mozzi and Warren [17] predicts two more distances (4.15 and 5.12 Å) but the small shoulders observed at 3.7 Å in the experimental atomic pair distribution function ($W(r)$) cannot be explained by this structural model. Another approach has been proposed by Bell and Dean [19] for the structure of amorphous SiO_2. They constructed a *physical model*. This theoretical model provides information about the local environement of the silicon atoms inside the continuum random networks. The total radial distribution function, $W(r)$, derived from this geometrical model indicates a strong correlation between the theoretical approach and our experimental $W(r)$ functions of these nanocomposites.

The comparison between theoretical and experimental atomic distribution functions, $W(r)$, demonstrates that all the different peak positions, even the peak at $r = 3.7$ Å match. In the refined model structure by Gaskell *et al.* [20], this peak (3.7 Å) was predicted to be more pronounced as observed in our experimental $W(r)$ (Fig. 4). The calculated density is the same as the assumed one used for obtaining a slope of (-1) before the first peak of $W(r)$. The density obtained in the Bell and Dean model is $1.99\ g \cdot cm^{-3}$ and the estimated density used in this work is $2.00\ g \cdot cm^{-3}$. This value is much less than that of crystalline cristobalite or tridymite ($2.32\ g \cdot cm^{-3}$ and $2.26\ g \cdot cm^{-3}$, respectively) or even amorphous structures which are generally in the range of 2.15 to $2.20\ g \cdot cm^{-3}$. It means that silica obtained by the sol-gel process inside these nanocomposites is porous. The average coordination number of the first atomic shell using this estimated density is 3.8–4.0.

By comparing the theoretical and experimental $W(r)$, it can be concluded that all maxima are attributed to the bond length of the SiO_2 phase. The following arguments demonstrates why the radial distribution functions do not reveal any structural information on the second phase (polymer). The absence of the structural (atomic arrangement) information of this phase could be explained by very high mobility of polymer. Such a liquid like character (disorded) has been previously identified by ^{13}C NMR reported in previous work [8]. Hence, the polymer phase has a disordered atomic arrangement with an unknown degree of disorder. On the other hand, it is well known that in periodic substances, maximum structural information can be deduced from the Patterson distribution $[P(r)]$. In case of disordered material it is reduced to the atomic distribution. If distributions were perfectely disordered, $[P(r)]$ would *be equal to unity* and *no peaks will be present*, as in the case of perfect gases. In the case of real material with disordered atomic arrangements, the average scattered intensity, I, of 'N' randomly oriented molecules is obtained by the Debye formula. It is well known that the double summation is taken over all atom pairs. This signifies that in, for example in bulk polymers, we should take $f^2_{C-C} = 36$ and for the Si–O pairs in the grains $f^2_{Si-O} = 196$. Thus, the absence of structural information about the atomic arrangement (structure) of this very disordered phase can be explained by the significant difference of "f^2_{C-C}" and "f^2_{Si-O}" [21]. Hence the short range order is not revealed in the peak and is not observed beside the $W(r)$ of the silica phase.

3.2.3. ^{29}Si NMR

The results obtained from NMR spectroscopy would also provide a better understanding of the behaviour of polymers (PEG) inside such blends (see section and ref. [4] and [5]).The *ideal* silica random network is characterized by Si atoms surrounded by four oxygens, which are themselves bridging atoms in between two silicon atoms ($Si^*(OSi)_4$ units; Q^4 in NMR terminology). In these ideal CRN, oxygen's atoms bridge between two silicon atoms, which means there are some possibilities to deviate from an ideal network through *positional disordering*. Moreover, point defects such as broken bonds could be also observed leading to *compositional disordering*. Therefore, ^{29}Si solid state NMR is a powerful technique to describe the local environment of the silicon atoms inside these kinds of disordered networks. Fig. 5 presents the MAS-^{29}Si NMR spectra of materials H_{200} and N_{200} obtained using the CP and HP decoupling modes. On both spectra, two wide signals centred around −101 ppm and −111 ppm are observed. These signals are characteristic of Q^3 (three bridging oxygens; $XOSi^*(OSi)_3$, $X = H$ or C) and Q^4 (four bridging oxygens; $Si^*(OSi)_4$) environments [22].

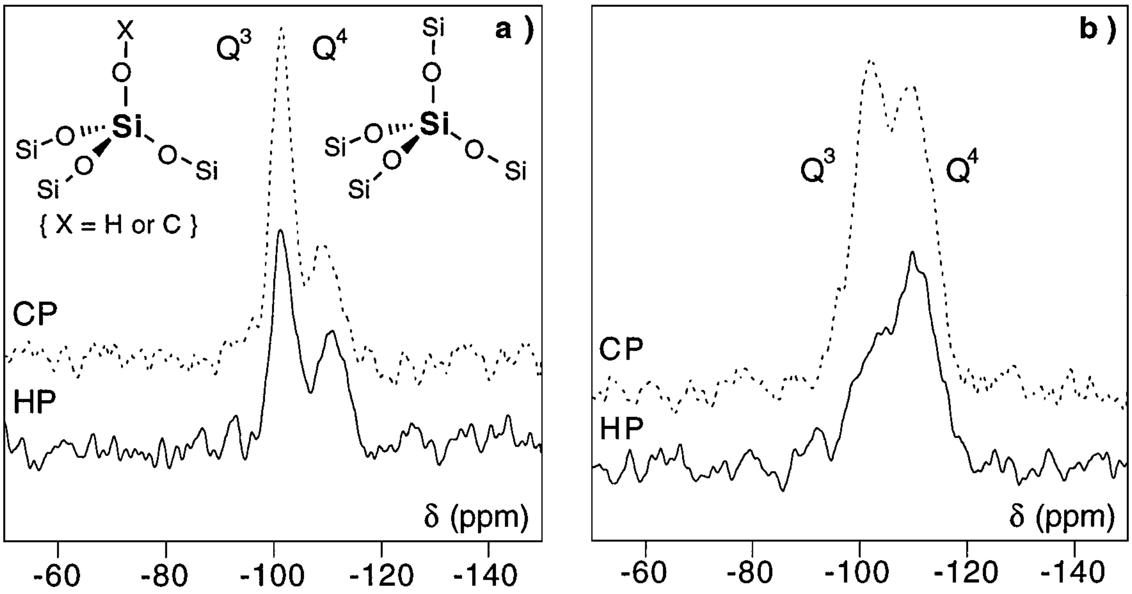

Figure 5 ^{29}Si MAS NMR spectra of a) H.$_{200}$; b) N.$_{200}$ samples obtained in CP (top) and HP (bottom) decoupling mode.

TABLE II ^{29}Si MAS-NMR spectroscopy: results of the deconvolution of HP decoupled and CP decoupled spectra for H.$_{200}$ and N.$_{200}$ nanocomposite materials

TEOS catalyst	^{29}Si-{^{1}H} decoupling mode	Q^3 linewidth	Q^4 linewidth	Area Q^3/Q^4	Degree of condensation
HCl	HP-DEC	170	270	1.5	85
HCl	CP	170	290	3.0	
NH$_4$F	HP-DEC	930	520	0.7	90
NH$_4$F	CP	500	600	1.0	

The presence of these two different families of sites implies that the atomic structures of these grains deviate from the perfect compositional order of an ideal CRN. In the acidic catalyzed sol-gel materials, defect points such as dead-ended bonds with hydroxy or alkoxy groups are present inside the silica network. The signals were deconvoluted with two Lorentzian shaped signals and the results of the data treatments are summarized in Table II.

In both samples, the ratio Q^3/Q^4 is larger for CP decoupled experiments than for HP decoupling conditions. CP enhances the magnetization of the rare ^{29}Si spin from that of the abundant ^{1}H spins of the polymer. However, the efficiency of this transfer precludes the proximity of the two phases, meaning that principally silicon atoms near the interface of polymer (PEG) and SiO$_2$ grains are probed by this technique. On the contrary, the low spatial selectivity of the high-power (HP) radio frequency decoupling allows complete visualization of the chemical structure of the silica aggregates. The comparison of HP and CP decoupling experiments thus proves to be a useful way to distinguish between silicon atoms at the silica-polymer interface and those of the core of the SiO$_2$ aggregates [23].

Larger Q^3/Q^4 ratio and important differences between HP and CP decoupling modes were measured for the acidic catalyzed materials, probing the large specific surface of these aggregates. These measurements demonstrate that the lower degree of condensation of the silicon atoms inside these materials and the corresponding silica aggregates could be described in terms of divided materials with larger specific surface. Conversely, more numerous Q^4 sites and wider signals were observed inside nucleophilic catalyzed materials. This is related to the more compact nanograins of these silica aggregates and the lower specific surface [24].

These results are in accord with those already discussed in previous papers in which the properties of the PEG phase are described on the basis of NMR, EPR (electron paramagnetic resonance) and DSC (differential thermal analysis) methods [6, 8]. These experiments point out the dynamical inhomogeneity of the polymer phase. On spectroscopic timescales (NMR and EPR), most of the polymer segments have reorientational rates similar to the those of the liquid polymers. Only the segments which are near the silica surface show restrained mobility, which is related to the possible formation of hydrogen bonds between both phases. PEG polymer chains that resemble a super-cooled liquid, then run into the voids, fill them tightly and become intermixed with the covalent grains in which sample form an ideal nanocomposite.

Such materials prepared under acidic catalysis are transparent. They present more compositional defects and their Guinier patterns show a tiny peak prior to the principal peak.

The origin of such a pre-peak in X-ray diffraction techniques, as an evolution of amorphous structure, is a difficult aspect of structural study in disordered material. However, alike evolution is an indication of medium range correlation or geometrical inhomogeneity. In acidic prepared materials, the correlation length was found to be 28 Å, which corresponds to the regions of compositional disorder (non stoichiometric composition and chemical inhomogeneity). The interpretation could be true since the prepeak cannot be observed in the Guinier patterns of materials prepared with NH$_4$F

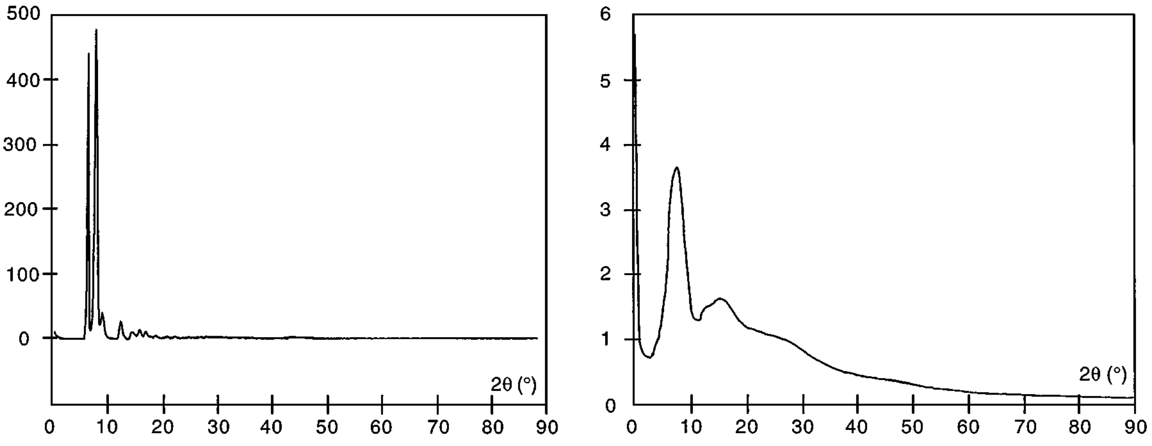

(a)

(b)

Figure 6 Amorphous diffractometry: Deconvolution of the X-ray pattern (Fig. 2) of solid PEG_{1000} recorded at room temperature ($T = 22\,^{\circ}C$). These two X-ray diagrams are numerically resolved from X-ray pattern of solid PEG_{100} (Fig. 2) into broad diffuse ring spectrum (a) and sharp line spectrum (b). Fig. 6a indicates similarity with liquid PEG polymer and nanocomposite (Fig. 2a,c).

as a catalyst and their NMR spectrum indicates a more compositional ordering (see Fig. 1).

The arguments and results discussed in previous section explain the absence of the structural information in the second phase (PEG) of the RDF, ($W(r)$) and also explain the usage of the NMR technique for completion of structural information associated to these blends.

Nevertheless, in order to acquire direct information about the polymer (PEG) phase, it is necessary to introduce another analytical method. The anomalous diffractometry technique was used to study the structure of the PEG (polymer) inside the voids of nanocomposites and an analogy between the x-ray patterns of nanocomposites and pure, PEG, in the form of liquid and solid was made. Fig. 2b shows that the x-ray diffraction patterns of nanocomposites do not have any Bragg reflection similar to the x-ray patterns of pure solid PEG. The superimposition of lines on halos (Fig. 2a) illustrates that the second phase PEG (polymer) in the nanocomposites do not have the same atomic arrangements as solid PEG (polymer). On the other hand, the x-ray patterns of solid PEG demonstrate the same features as any other polymer x-ray diagram, in which lines are superimposed on rings. By the separation procedures described by Laridjani [12, 25], these diffraction patterns have been numerically resolved into rings and sharp lines using computer analysis. Fig. 6a and b show, respectively, the ring diagram and the line spectrum of pure solid PEG. The comparison of x-ray pattern of the ring diagram i.e. the coherent background with the x-ray pattern of liquid PEG (polymer) may show, at first approximation disordered atomic arrangements. The analysis of the interference function, derived from ring diagrams of pure solid PEG, resulted in radial distribution functions (see details at ref. [12] and [25]), $W(r)$, with *only* three maxima at 1.30, 2.4 and 3.2 Å. These maxima can be attributed to the short range order of disordered part of polymer. None of the interatomics distance of C–C distances in the PEG chains does not appear in the $W(r)$ of samples obtained under acidic catalysis.

Nevertheless, the $W(r)$ of other types of sol-gel materials, prepapred under the NH_4F condition, indicates the small distance of 2.6 Å. The latter can probably be associated to the C1–C3 = 2.6 Å of the polymer chain. This result has to be treated with reservation due to the limitation in the structural information. The x-ray diffraction confirmes that second phase (polymer) in two types of sol-gel materials are different in their morphology. The $W(r)$ curves derived from the $F(K)$ of sol-gel acquired under acidic conditions, present only the characteristic distance of the silica aggregates. Thus, it appears that in such diphasic materials, the second phase (the PEG component), is not observable. Although, the $W(r)$ of materials, observed under the NH_4F condition, does not behave in the same fashion.

Despite the above analogies, other methods such as anomalous scattering effects or neutron diffraction (by replacing hydrogen by deuterium) should be utilized so that the behaviour of the second phase polymer could be understood in detail. These methods change the contrasts between the different components of these types of material (work in progress). They would permit us to obtain more precise information about SRO and medium range order of polymer chains in pores.

4. Conclusion

The X-ray diffraction techniques determined the presence of SiO_2 grains in silica-PEG nanocomposites. The positional ordering (geometrical ordering) of these grains corresponds to the ideal continuum random network and not to the microcrystallites. The compositional ordering, measured by NMR spectroscopy suggests the existence of two kinds of silicon atoms inside the silica grains. NMR suggests the existence of two kinds of silicon atoms inside the grains of SiO_2. One type corresponds to the complete silica coordination shell (Q^4 species), while the other type corresponds to point defects where one of the oxygens is bonded to hydrogen or carbon atoms (Q^3 species). In this work, this type of material has been considered as an ideal nanocomposite.

For both materials, like in all the crystalline or amorphous silica structure, a perfect tetrahedron is the baisc unit of the silica aggregates. The total distribution function, $W(r)$, derived from the geometrical Bell and Dean's model indicates a strong correlation between the theoretical approach and the experimental $W(r)$ function of these nanocomposites.

The absence of second polymeric phase can be interpreted as follows: the long polymer chains travelling in the void do not have particular time or condition to possess a periodic structure. They are in void with very high degree of disorder as an interface between the grains. This results in having very diffusive rings for such disordered as an interface between the grains.This results in having very diffusive rings for such disordered chains of light atoms. Their contrast relative to the scattering of SiO_2 grains is not enough to be observed on the same diagram.

Acknowledgements

We are grateful to Dr. F. Dénoyer for useful discussions. We thank Mr. J. P. Wagner for his technical assistance. Much help was received from different companies such as the "Development Analyses and Measures" and "Maison Internationale de l'Information". We thank them for their generous technical assistance. Finally, the realisation of this X-ray complex would not have started without Dr. S. Megtert providing funds for it.

References

1. a) *Mat. Res. Soc. Symp. Proc.*, Vol. 346: "Better Ceramics Through Chemistry VI," edited by A. K. Cheetham, C. J. Brinker, M. L. McCartney, 1994; b) *Mat. Res. Soc. Symp. Proc.*, Vol. 435: "Better Ceramics Through Chemistry VII," edited by A. K. Cheetham, C. J. Brinker, M. L. McCartney, 1996; c) "Hybrid Organic-Inorganic Materials," edited by C. Sanchez and F. Ribot, *New J. Chem.*, **18**, 1994; d) "Hybrid Organic-Inorganic Composites," edited by J. E. Mark, C. Y.-C. Lee, P. A. Bianconi, ACS Symp. Ser., 585, 1995.
2. a) B. M. NOVAK, *Adv. Mat.* **5** (1993) 422; b) C. SANCHEZ and F. RIBOT, *New J. Chem.* **18** (1994) 1007; c) P. JUDEINSTEIN and C. SANCHEZ, *J. Mater. Chem.* **6** (1996) 511.
3. C. J. T. LANDRY, B. K. COLTRAIN, M. R. LANDRY, J. J. FITZGERALD and V. K. LONG, *Macromolecules* **26** (1993) 3712.
4. I. A. DAVID and G. W. SCHERER, *Chem. Mater.* **7** (1995) 1957.
5. D. E. RODRIGUES, A. B. BRENNAN, C. BETRABET, B. WANG and G. L. WILKES, *ibid.* **4** (1992) 1437.
6. P. JUDEINSTEIN, J. TITMAN, M. STAMM and H. SCHMIDT, *ibid.* **6** (1994) 127.
7. A. GUINIER and D. L. DEXTER, "X-Rays Studies of Materials" (Interscience Publishers, J. W., 1963).
8. P. LESOT, S. CHAPUIS, J. P. BAYLE, J. RAULT, E. LAFONTAINE, A. CAMPERO and P. JUDEINSTEIN, *J. Mater. Chem.* **8** (1998) 147.
9. a) M. LARIDJANI, P. LEBOUCHER and J. F. SADOC, *Spectra 2000* **16**(128) 1988. b) M. LARIDJANI and J. F. SADOC, *J. Phys. France* **48** (1987) 114.
10. A. GUINIER and G. FOURNET, "Small-Angle Scattering of X-ray" (Wiley, New York, 1955).
11. M. LARIDJANI, J. P. POUGET, E. M. SCHERR, A. G. MACDIARMID, M. E. JOZEFOWICZ and A. J. EPSTEIN, *Macromolecules* **25** (1992) 4106.
12. M. LARIDJANI and J. EPSTEIN, *Eur. Phys. J.*, **B7** (1999) 585.
13. B. E. WARREN and R. L. MOZZI, *Acta Cryst.* **21** (1966) 459.
14. A. C. WRIGHT, *J. Non-Cryst. Solids* **179** (1994) 84.
15. H. F. POULSEN, J. NEUEFEIND, H.-B. NEUMANN, J. R. SCHNEIDER and M. D. ZEIDLER, *ibid.* **188** (1995) 63.
16. H. OHSAKI, K. MIURA, A. IMAI, M. TADA and M. A. AEGERTER, *J. Sol-Gel Sci. & Tech.* **2** (1994) 245.
17. R. L. MOZZI and B. E. WARREN, *J. Appl. Cryst.* **2** (1969) 169.
18. E. H. HENNINGER, R. C. BASCHERT and L. HEATON, *J. Phys. Chem. Solids* **28** (1967) 423.
19. R. J. BELL and P. DEAN, *Phil. Mag.* **25** (1972) 1381.
20. P. H. GASKELL and I. D. TARRANT, *Phil. Mag. B* **42**(2) (1980) 265.
21. A. GUINIER, "Théorie et Technique de la Radiocristallographie," 3rd. ed. (Dunod, Paris, 1964).
22. a) G. ENGELHARDT "High-Resolution Solid-State NMR of Silica and Zeolites" (Wiley, New York, 1987) p. 76; b) R. K. HARRIS and R. H. NEWMAN, *J. Chem. Soc., Faraday Trans.* **73** (1977) 1204.
23. C. C. LIU and G. E. MACIEL, *J. Amer. Chem. Soc.* **118** (1996) 5103.
24. F. DEVREUX, J. P. BOILOT, F. CHAPUT and A. LECOMTE, *Phys. Rev. A* **41** (1990) 6901.
25. M. LARIDJANI, *J. Phys I, France* **6** (1996) 1347.

Received 11 June
and accepted 11 June 1999